ELSEVIER

Journal of Quantitative Spectroscopy & Radiative Transfer 109 (2008) 1496–1503

Journal of Quantitative Spectroscopy & Radiative Transfer

www.elsevier.com/locate/jqsrt

Correction factors for a total scatter/backscatter nephelometer

Arturo Quirantes[a,*], Francisco J. Olmo[a,b], Hassan Lyamani[a,b], Lucas Alados-Arboledas[a,b]

[a]*Department of Applied Physics, University of Granada, 18071 Granada, Spain*
[b]*Centro Andaluz de Medio Ambiente (CEAMA), Avenida del Mediterráneo s/n, 18071 Granada, Spain*

Received 16 October 2007; accepted 17 December 2007

Abstract

Total aerosol scattering and backscattering atmospheric values are typically obtained with an integrating nephelometer. Due to design limitations, measurements do not cover the full (0°–180°) angular range, and correction factors are necessary. The effect of angle cutoff is examined for a number of particle size distributions and refractive indices. Scattering data for sub-micron particles can be corrected by the use of a modified Anderson approximation, while data for larger particle distributions can be approximated by a function of the effective size parameter. Correction factors for the hemispheric backscatter ratio are found to be small if nonsphericity is assumed. Such approximations will help more accurate corrections for angle range, particularly at large size parameter values.

Keywords: Light scattering; Atmospheric aerosols; Nephelometer; Anderson approximation

1. Introduction

Atmospheric aerosol particles have a significant impact on the Earth's radiation budget and on regional air pollution (visibility, photochemistry, health effects,…). In contrast to greenhouse gases, aerosol particles have variable optical properties that must be studied in the field. The atmospheric aerosol effects can be direct (scattering and absorbing incoming solar radiation) or indirect (performing as cloud condensation nuclei and varying the microphysical and lifetime of clouds). Indeed, atmospheric aerosol particles are one of the greatest sources of uncertainty in the assessment of global climate forcing [1,2].

To determine the aerosol influence on climate, visibility, and photochemistry, several key aerosol properties are required. These include the aerosol light extinction, single-scattering albedo, and optical depth, among others. The variety of chemical and physical forms exhibited by aerosol particles, as well as their short atmospheric lifetime, dictate measurements of their properties across a wide range of locations and timescales. Atmospheric aerosols have a significant impact on regional air pollution as well as on the radiation budget. To determine its influence on climate, visibility, and photochemistry, several key aerosol properties are required. These include the aerosol light extinction, single-scattering albedo, and optical depth, among others.

*Corresponding author.
E-mail address: aquiran@ugr.es (A. Quirantes).

0022-4073/$ - see front matter © 2007 Elsevier Ltd. All rights reserved.
doi:10.1016/j.jqsrt.2007.12.014

Integrating nephelometers, such as the TSI 3563, are particularly well suited to measure optical properties of the atmosphere like scattering and backscattering coefficients $\sigma(\lambda) = N\langle C_{\mathrm{sca}}\rangle$, $\beta(\lambda) = N\langle C_{\mathrm{back}}\rangle$, where $\langle C_{\mathrm{back}}\rangle$ is the size-averaged scattered intensity in the backward hemisphere. Scattering data, typically obtained at three wavelengths (450, 550, 700 nm) can be extrapolated to other wavelengths by the use of the wavelength-dependent Ångström exponent $\mathring{A}$ [3]:

$$\sigma(\lambda) = C\lambda^{-\mathring{\mathrm{A}}}. \tag{1}$$

An Ångström exponent between two wavelengths can be experimentally obtained as

$$\mathring{\mathrm{A}}(\lambda_1, \lambda_2) = -\frac{\mathrm{Log}(\sigma(\lambda_1)/\sigma(\lambda_2))}{\mathrm{Log}(\lambda_1/\lambda_2)}. \tag{2}$$

The scattering and backscattering coefficients measured with a nephelometer require corrections due to a number of factors. Relative humidity can influence calibration values based on dry, standard gases. The effect of photon counting must be also taken into account, as well as wavelength sensitivity. Additional imperfections of the nephelometer, such as the backscatter shutter not separating light at exactly 90°, is also a relevant factor [4,5]. But even a perfectly built and calibrated nephelometer will suffer from a basic design drawback: angular integration is limited to the 7°–170° range. The scattering and backscattering coefficients are, therefore, undervalued, since the forward (0°–7°) and backward (170°–180°) peaks are removed.

Several approaches have been proposed. The missing peaks can be calculated and added, but it requires prior knowledge about the particle size distribution, as well as previous assumptions regarding shape and composition [6]. An alternative method calls for the construction of a synthetic phased function that combines experimental data and calculation of the forward and backward peaks under the assumption of an equal-projected-area particle size distribution of spheres. This approach has been used to process laboratory measurements of one of the Amsterdam database aerosols [7,8], a quartz aerosol whose phase function was measured in the angle interval 5°–173°.

One of the most popular correction mechanisms, put forward by Anderson and Ogren [2], involves the parametrization of the correction factor for scattering (the ratio between full and truncated scattering cross sections) in terms of the experimentally determined Ångström exponent $\mathring{A}$ (Eq. (1)). A close look reveals that the Anderson approximation is limited to particle size distributions with a single width and a limited set of refractive indices and mean diameter. A full coverage variation of mean radius is lacking, relying instead in two different population models, sub-micron (effective size parameter $x_{\mathrm{eff}} = 3$–6) and super-micron ($x_{\mathrm{eff}} = 30$–55). The effect of nonsphericity is not taken into account but assumed to be negligible on the premise that scattering in the near-forward direction is insensitive to shape effects.

In the present work, the validity of the Anderson approximation is checked by direct comparison to computer simulations of light scattering quantities by particle size distributions of spheres and randomly oriented spheroids (oblate and prolate). New correction factors are suggested for sub-micron particles. For larger (micron-sized) particles, where the Anderson approximation is known to yield less accurate results, an approximation is suggested whereby the correction factor can be written as a simple function of the effective size parameter. The behavior of backscattering corrections is briefly outlined.

2. Theory

Light scattering properties were calculated for five values of the refraction index m: 1.33, 1.46, $1.55 + i0.001$, $1.6 + i10^{-5}$, $1.6 + i0.6$. Mie theory was used for spherical particles [9,10], and the T-matrix method yielded calculations on randomly oriented spheroids [11,12] with an axial ratio (long to short axis ratio) $\varepsilon = 1.8$. Correction factors were obtained by subtracting the forward (0°–7°) and backward (170°–180°) contributions from the full integrals, e.g.:

$$C^{*}_{\mathrm{sca}} = \frac{1}{2} C_{\mathrm{sca}} \left(1 - \int_{0^\circ}^{7^\circ} p(\theta) \sin\theta \, \mathrm{d}\theta - \int_{170^\circ}^{180^\circ} p(\theta) \sin\theta \, \mathrm{d}\theta \right). \tag{3}$$

Table 1
Maximum effective size values for light-scattering computations of spheroids (oblate and prolate) with an axial ratio $\varepsilon = 1.8$

v_{eff}	0.01	0.1	0.2	0.5	1	2	3	5
x_{eff}	54	39	33	23	16	11	8	5

and likewise, for backscattering cross section. Single-scattering results were then size-averaged by assuming a power-law particle size distribution (PSD)

$$n(x) = \begin{cases} Cx^{-3} & x_1 \leqslant x \leqslant x_2, \\ 0 & \text{otherwise}, \end{cases} \tag{4}$$

where x stands for the equal-projected-area size parameter. Correction factors were defined as the size-averaged full-to-truncated ratios for the scattering cross section $\langle C_{\text{sca}} \rangle$ and for the hemispheric backscatter ratio $\langle b \rangle = \langle C_{\text{back}} \rangle / \langle C_{\text{sca}} \rangle$:

$$F_{\text{s}} = \frac{\langle C_{\text{sca}} \rangle}{\langle C^*_{\text{sca}} \rangle} = \frac{\int_{0^\circ}^{180^\circ} p(\theta) \sin\theta \, \mathrm{d}\theta}{\int_{7^\circ}^{170^\circ} p(\theta) \sin\theta \, \mathrm{d}\theta},$$
$$F_{\text{b}} = \frac{\langle b \rangle}{\langle b^* \rangle} = \frac{\int_{90^\circ}^{180^\circ} p(\theta) \sin\theta \, \mathrm{d}\theta / \int_{0^\circ}^{180^\circ} p(\theta) \sin\theta \, \mathrm{d}\theta}{\int_{90^\circ}^{170^\circ} p(\theta) \sin\theta \, \mathrm{d}\theta / \int_{7^\circ}^{170^\circ} p(\theta) \sin\theta \, \mathrm{d}\theta}. \tag{5}$$

An Ångström exponent was calculated as in Eq. (2), for λ_1, $\lambda_2 = 450$, 700 nm. Particle size distributions $p(x)$ have been parameterized by using the effective size parameter x_{eff} and effective variance v_{eff}:

$$x_{\text{eff}} = \frac{\int_{x_1}^{x_2} x^3 p(x) \, \mathrm{d}x}{\int_{x_1}^{x_2} x^2 p(x) \, \mathrm{d}x}, \quad v_{\text{eff}} = \frac{\int_{x_1}^{x_2} x^2 (x - x_{\text{eff}})^2 p(x) \, \mathrm{d}x}{x_{\text{eff}}^2 \int_{x_1}^{x_2} x^2 p(x) \, \mathrm{d}x}, \tag{6}$$

thus following Hansen and Travis' suggestion that scattering properties of most plausible PSDs depend on those two parameters, actual shape being of minor importance [13].

In the present work, the maximum x_{eff}, v_{eff} values have been set to 100 and 5, respectively. Large as they might seem, they are sometimes found airborne, for instance as the combustion products of powdered coal near a power plant, or in the aftermath of large volcanic eruptions [7]. In the case of nonspherical particles, where an accuracy of 10^{-5} for the calculation of cross sections [14] was set, convergence limitations in the T-matrix method force a maximum monodisperse, equal-projected-area size parameter in the vicinity of $x = 62$. All comparisons made between spherical and spheroidal particles in this work are to be considered valid only within the limiting values of x_{eff} as Table 1 shows.

3. Results and discussion

It has been previously shown [4,15] that, in the case of sub-micron particles, the relationship between the correction factor and the Ångström exponent $\mathring{A}$ is strong and lineal, with a weak dependence on either refractive index or particle composition. On the other hand, for small $\mathring{A}$ values (large particles), the correction factor grows larger while the F_{s}–$\mathring{A}$ relationship becomes weaker.

Calculated values of the correction factor for a refraction index $m = 1.55 + \text{i}0.001$ is shown in Fig. 1. In the region of small particle size ($\mathring{A} = 1$–3), F_{s} has a lineal dependence on $\mathring{A}$, which is nearly insensitive on PSD width. Lineal fits, shown in Table 2, are valid within the range $\mathring{A} = 0.5$–3. For the smallest particles ($\mathring{A} = 3$–4), a constant correction value $F_{\text{s}} = 1.01717$ (Rayleigh limit) can be used. No lineal fitting was feasible in the case of strong absorption ($m = 1.6 + \text{i}0.6$). The correction factor was then smaller than in the case of less absorbing material, having values between 1.015 and 1.03 in the $\mathring{A} > 1$ region.

Since the forward peak, which is primarily responsible for the correction factor, is nearly insensitive to particle shape, the effect of shape is expected to be small. Correction factors calculated for oblate particles are virtually identical to those for prolate spheroids with the same axial ratio and projected area, and are similar

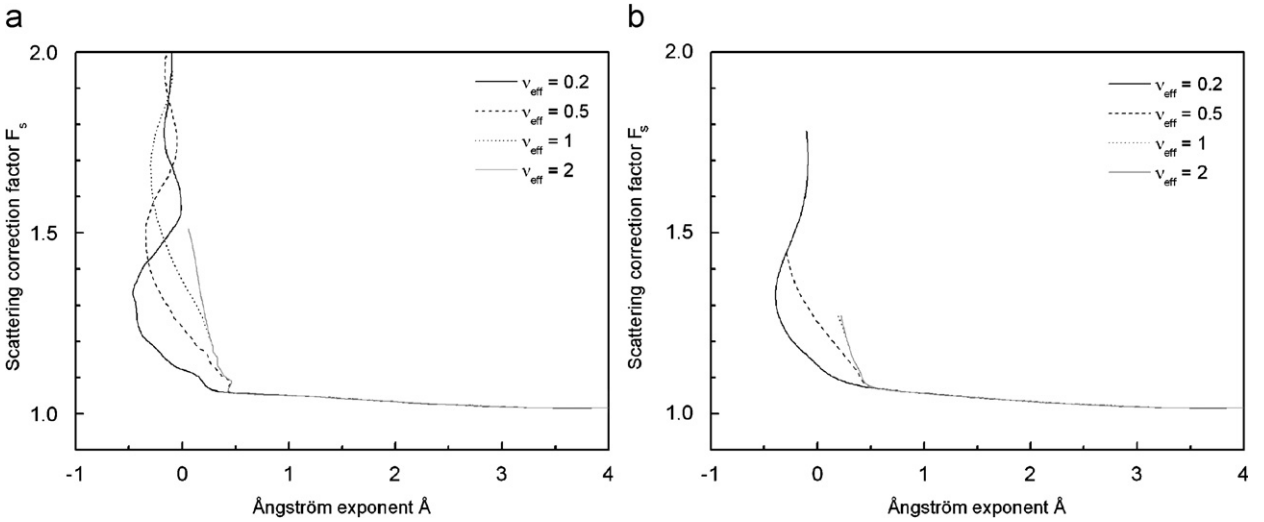

Fig. 1. Scattering correction factors for (a) spheres, (b) oblate spheroids ($\varepsilon = 1.8$), for several values of the particle size distribution width, and index of refraction $m = 1.55 + i0.001$.

Table 2
Fitting parameters for the Anderson approximation $F_s = a + b\mathring{A}$ for spheres and spheroids with an axial ratio $\varepsilon = 1.8$, and validity range

m	a	b	
1.33	1.160	−0.049	Spheres
	1.182	−0.058	Spheroids
1.46	1.087	−0.023	Spheres
	1.102	−0.028	Spheroids
1.55 + i0.001	1.067	−0.016	Spheres
	1.080	−0.021	Spheroids
1.6 + i0.00001	1.060	−0.014	Spheres
	1.070	−0.018	Spheroids

v_{eff}	0.1	0.2	0.5	1	2
x_{eff}	1.5–3.9	1.2–3.7	0.7–3.5	0.5–2.5	0.4–1.6

(within 1–2%) to results obtained for equal-projected-area spheres within the size range outlined in Table 2, for all five refractive indices used in the present work, and for all but the narrowest size distributions ($v_{eff} \leqslant 0.2$). This shape insensitivity extends to the micron-size zone, supporting the view that particle distributions of interest can be regarded as spherical as far as correction factors for scattering is concerned.

As particle sizes get larger, the relation between F_s and $\mathring{A}$ is no longer lineal. The correction factor shows a strong dependence on PSD width and particle composition, and the curve becomes multivalued for all but the most absorbing particles. A correlation between F_s and the effective size x_{eff} becomes can be used. $F_s - x_{eff}$ curves are univalued, their behavior allows for a simple lineal (quadratic, in the case of heavy absorption), or logarithmic, fit.

A set of best-fit curves has been obtained for each m value by dividing the entire size interval ($x_{eff} = 0$–100) into a small number of sub-intervals. Fitting coefficients, as well as their size range validity, are shown in Tables 3–7, and reproduce the exact correction factor to within 1% or less in most PSDs examined. For

Table 3
Correction factors for scattering as a function of the effective size parameter x_{eff}, for an index of refraction $m = 1.33$

v_{eff}	$F_s = a + bx_{eff}$	$F_s = a + b\,\mathrm{Ln}(x_{eff})$	$F_s = a + b\,\mathrm{Ln}(x_{eff})$
0.2	(0.993, 0.024) [1–12]	(0.134, 0.467) [12–33]	(1.099, 0.200) [33–100]
0.5	(1.025, 0.020) [0.8–18]	(0.196, 0.400) [18–70]	(1.121, 0.180) [65–100]
1	(1.232, 0.006) [15–70]	(1.035, 0.095) [0.7–15]	(−0.056, 0.401) [60–100]
2	(1.005, 0.063) [0.4–2]	(1.038, 0.120) [2–20]	(1.138, 0.074) [20–100]
3	(1.011, 0.076) [0.3–2.5]	(1.086, 0.113) [2.5–18]	(1.174, 0.079) [18–100]
5	(1.012, 0.111) [0.2–1.5]	(1.132, 0.113) [1.5–12]	(1.231, 0.072) [12–100]

Fitting parameters are given in parenthesis; size range validity is given in brackets.

Table 4
Same as Table 3, for $m = 1.46$

v_{eff}	$F_s = a + bx_{eff}$	$F_s = a + b\,\mathrm{Ln}(x_{eff})$	$F_s = a + b\,\mathrm{Ln}(x_{eff})$
0.2	(1.005, 0.005) [1–9]	(0.221, 0.435) [9–40]	(1.199, 0.172) [40–100]
0.5	(1.012, 0.019) [0.8–25]	(0.237, 0.388) [25–60]	(0.863, 0.235) [60–100]
1	(1.007, 0.030) [0.6–2.5]	(0.963, 0.118) [2.5–30]	(0.224, 0.335) [30–100]
2	(1.013, 0.041) [0.5–2]	(1.014, 0.112) [2–10]	(1.085, 0.083) [10–100]
3	(1.008, 0.060) [0.3–2]	(1.048, 0.111) [2–10]	(1.133, 0.075) [10–100]
5	(1.015, 0.080) [0.2–2]	(1.095, 0.108) [2–10]	(1.177, 0.071) [10–100]

Table 5
Same as Table 3, for $m = 1.55 + i0.001$

v_{eff}	$F_s = a + bx_{eff}$	$F_s = a + b\,\mathrm{Ln}(x_{eff})$	$F_s = a + b\,\mathrm{Ln}(x_{eff})$
0.2	(1.005, 0.015) [1–4]	(0.943, 0.028) [4–10]	(0.181, 0.465) [10–100]
0.5	(1.005, 0.020) [0.7–3]	(0.996, 0.021) [3–20]	(−0.109, 0.506) [20–100]
1	(1.010, 0.025) [0.5–7]	(1.127, 0.009) [7–40]	(−0.374, 0.505) [40–100]
2	(1.012, 0.036) [0.4–2]		(1.012, 0.107) [2–100]
3	(1.009, 0.052) [0.3–3]		(1.057, 0.102) [3–100]
5	(1.011, 0.074) [0.2–2.5]		(1.097, 0.102) [2.5–100]

Table 6
Same as Table 3, for $m = 1.6 + i0.00001$

v_{eff}	$F_s = a + bx_{eff}$	$F_s = a + b\,\mathrm{Ln}(x_{eff})$	$F_s = a + b\,\mathrm{Ln}(x_{eff})$
0.2	(0.978, 0.024) [1–9]	(0.224, 0.432) [9–40]	(1.207, 0.171) [40–100]
0.5	(1.003, 0.020) [0.8–16]	(0.308, 0.370) [16–70]	(0.986, 0.210) [70–100]
1	(1.010, 0.024) [0.6–5]	(0.949, 0.112) [5–22]	(0.287, 0.325) [22–100]
2	(1.007, 0.039) [0.4–2]	(1.007, 0.107) [2–10]	(1.063, 0.083) [10–100]
3	(1.007, 0.052) [0.3–2]	(1.041, 0.105) [2–10]	(1.110, 0.075) [10–100]
5	(1.007, 0.078) [0.2–1]	(1.086, 0.101) [1–10]	(1.157, 0.070) [10–100]

narrow size distributions ($v_{eff} = 0.2$) this difference increases to about 2%. In the case of small size paramater values, the Rayleigh theory yields an approximate value $F_s = 1.01717$, which is valid to a difference of 0.3%.

An example of the fitting procedure is shown in Fig. 2 for the case $m = 1.6 + i10^{-5}$ and $v_{eff} = 2$. Sometimes, the best-fit curves do not form a continuous graph in the entire size interval. The curves and size intervals have been chosen so as to allow for an efficient and simple fitting within each sub-interval. All fitting curves have

Table 7
Same as Table 3, for $m = 1.6 + i0.6$

v_{eff}	$F_s = a + bx_{eff} + cx_{eff}^2$	$F_s = a + b\,\mathrm{Ln}(x_{eff})$	$F_s = a + b\,\mathrm{Ln}(x_{eff})$
0.2	(1.018, 0, 0.005) [1–6]	(0.615, 0.094) [6–38]	(−1.584, 1.583) [38–100]
0.5	(1.000, 0.021, 0.003) [0.7–5]	(0.886, 0.058) [5–40]	(−5.398, 2.337) [40–100]
1	(0.991, 0.500, 0) [0.5–8]	(1.167, 0.029) [8–30]	
1		(1.280, 0.026) [30–100]	
2	(1.009, 0.026, 0.020) [0.3–2]	(1.704, 0.006) [60–100]	(0.940, 0.272) [2–60]
3	(1.003, 0.051, 0.027) [0.3–1.5]		(1.026, 0.263) [1.5–100]
5	(0.995, 0.114, 0.029) [0.2–1.5]		(1.135, 0.261) [1.5–100]

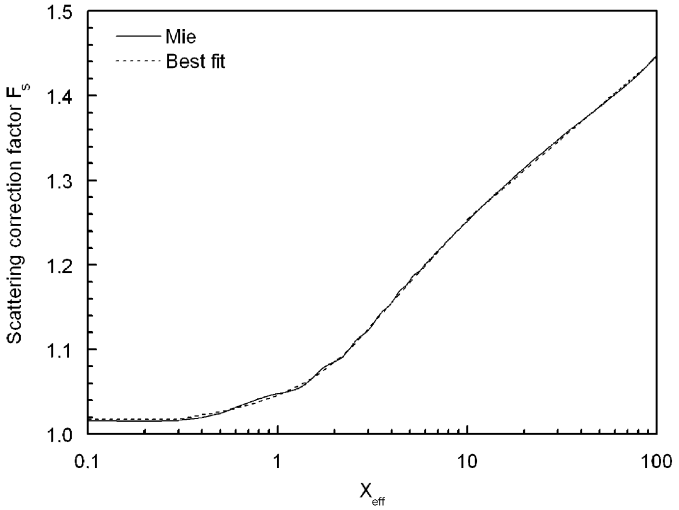

Fig. 2. Computed (Mie) value and best fit for the scattering correction factor for particle size distributions with a width $v_{eff} = 2$ and index of refraction $m = 1.6 + i10^{-5}$.

been carried out on spherical scatterers. The nearly independence of F_s on shape, previously outlined, allows results to stand valid also for nonspherical particles.

The choice of particle shape has deeper implication in the correction factor for backscattering. As the example in Fig. 3 shows ($m = 1.55 + i0.001$), the assumption of sphericity calls for high correction values in the zone of large particle size. On the other hand, the backscattering correction factor is closer to unity for spheroidal scatterers ($\varepsilon = 1.8$). In the small particle region, the $F_b - x_{eff}$ curve behaves in a similar way as in the spherical case, but for larger particles the correction factor takes values in the 1.01–1.02 range. In the case of nonabsorbing or weakly absorbing materials, the trend for large x_{eff} seems to be descending, but the size limitations outlined above prevents us from reaching any firm conclusion. For the absorbing case ($m = 1.6 + i0.6$), the curve tends to a constant value $F_b = 1.015$, which is itself weakly depending on m assuming its imaginary part is larger than about 0.5.

Taking into account the fact that spherical scatterers in nature are the exception rather than the norm, and that axial ratios of about 1.8 have been suggested for aerosol populations [16,17], our data suggest a correction factor of about 1.015 for the hemispheric backscatter ratio to account for the inevitable limitations in nephelometer angle acceptance. Only for the smallest size distributions is a larger value needed, as backscattering correction factor values slowly increase towards the Rayleigh limit 1.02314. It is therefore strongly advised not to carry out any backscattering correction based on Mie theory, unless particles are known to be spherical.

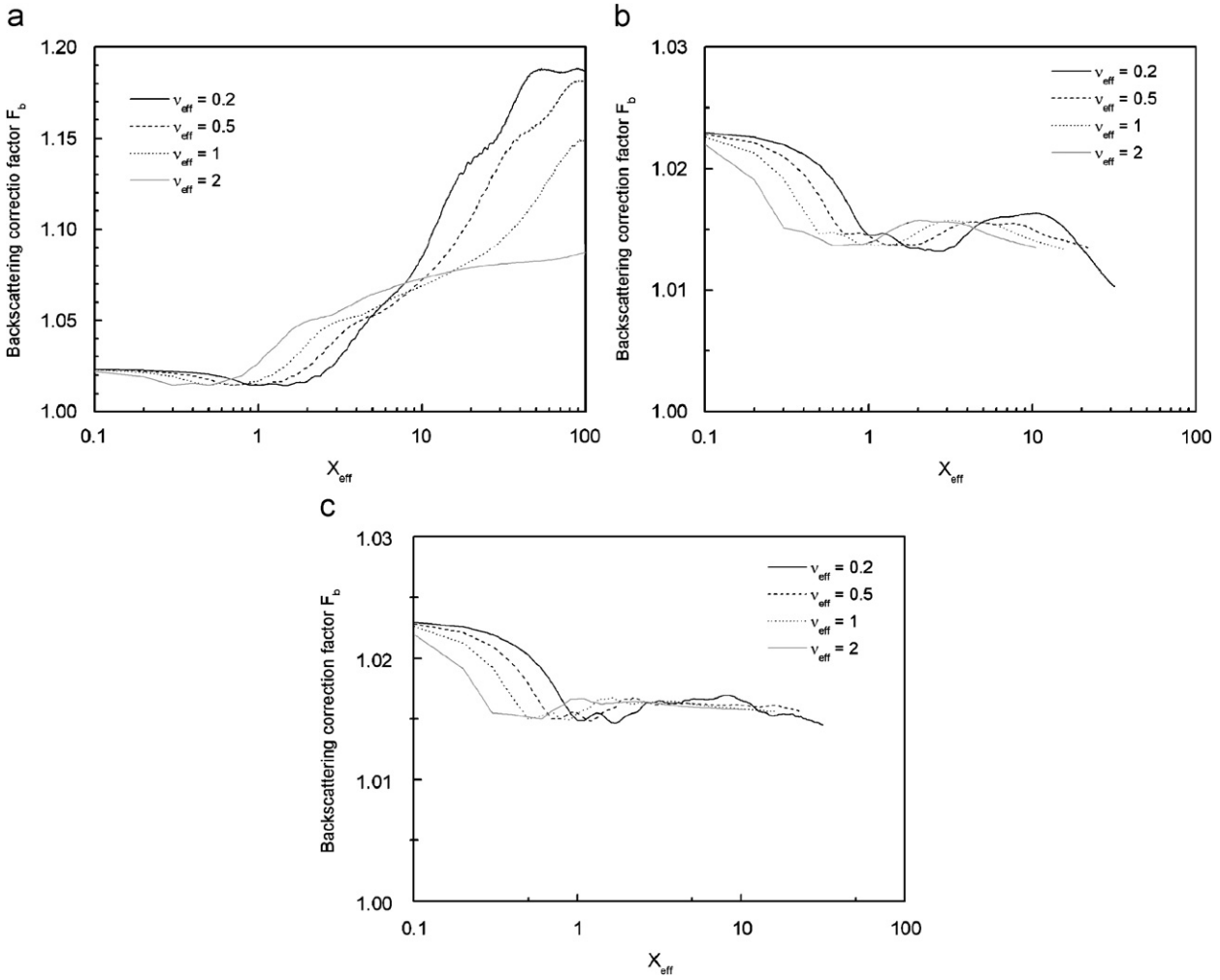

Fig. 3. Backscattering correction factors for (a) spheres, (b) oblate spheroids ($\varepsilon = 1.8$), (c) prolate spheroids ($\varepsilon = 1/1.8$), for several values of the particle size distribution width, and index of refraction $m = 1.55 + i0.001$.

Acknowledgment

Financial Support from Spain's Ministry of Science and Education, Projects CGL 2004-05984-C07-03, CGL 2007-66477-C02-01 and FIS 2005-06860-C02-01, is gratefully acknowledged.

References

[1] Intergovernmental Panel on Climate Change (IPCC) climate change 2001: the scientific basis. New York: Cambridge University Press; 2001.
[2] Ramanathan V, Crutzen PJ, Kiehl JT, Rosenfeld D. Aerosols, climate, and the hydrological cycle. Science 2001;249:2119–24.
[3] Ångström A. On the atmospheric transmission of sun radiation and on dust in the air. Geogr Ann 1929;11:156–66.
[4] Anderson TL, Ogren JA. Determining aerosol radiative properties using the TSI 3563 integrating nephelometer. Aerosol Sci Technol 1998;29:57–69.
[5] Anderson TL, Covert DS, Marshall SF, Laucks ML, Charlson RJ, Waggoner AP, et al. Performance characteristics of a high-sensitivity, three-wavelength total scatter/backscatter nephelometer. J Atmos Ocean Technol 1996;13:967–86.
[6] Olmo FJ, Quirantes A, Lyamani H, Alados-Arboledas L. Influence of particle shape on the integral scattering coefficiente of aerosol at Granada, Spain. J Aerosol Sci, submitted.

[7] Volten H, Muñoz O, Rol E, de Haan JF, Vassen W, Hovenier JW, et al. Scattering matrices of mineral aerosol particles at 441.6 and 632.8 nm. J Geophys Res 2001;106:17375–401 Amsterdan Light Scattering database available at http://www.astro.uva.nl/scatter/.
[8] Liu L, Mishchenki MI, Hovenier JW, Volten H, Muñoz O. Scattering matrix of quartz aerosols: comparison and synthesis of laboratory and Lorenz–Mie results. JQSRT 2003;79–80:911–20.
[9] Mie G. Beiträge zur Optik trüber Medien speziell kolloidaler Metallösungen. Ann Phys 1908;4:377–445.
[10] Bohren CF, Huffman DR. Absorption and scattering by small particles. New York: Wiley-Interscience; 1983.
[11] Waterman PC. Symmetry, unitarity, and geometry in electromagnetic scattering. Phys Rev 1971;D3:835–9.
[12] Mishchenko MI. Light scattering by randomly oriented axially symmetric particles. JOSA A 1991;8:871–82.
[13] Hansen JE, Travis LD. Light scattering in planetary atmospheres. Space Sci Rev 1974;16:527–619.
[14] Mishchenko MI. Light scattering by size–shape distributions of randomly oriented axially symmetric particles of a size comparable to a wavelength. Appl Opt 1993;32:4652–66.
[15] Nessler R, Weingartner E, Baltensperger U. Adaptation of dry nephelometer measurements to ambient conditions at the Jungfraujoch. Environ Sci Technol 2005;39:2219–28.
[16] Hill SC, Hill AC, Barber PW. Light scattering by size/shape distributions of soil particles and spheroids. Appl Opt 1984;23:1025–32.
[17] Mishchenko MI, Lacis AA, Travis LD. Nonsphericity of dust-like tropospheric aerosols: implications for aerosol remote sensing and climate modeling. Geophys Res Lett 1995;22:1077–80.